THE JOURNAL OF PHYSICAL CHEMISTRY Letters

pubs.acs.org/JPCL Letter

Exciton Spatial Dynamics and Self-Trapping in Carbon Nanocages

Beatriz Rodríguez-Hernández, Tammie Nelson, Nicolas Oldani, Aliezer Martínez-Mesa, Llinersy Uranga-Piña, Yasutomo Segawa, Sergei Tretiak, Kenichiro Itami, and Sebastian Fernandez-Alberti*

Cite This: J. Phys. Chem. Lett. 2021, 12, 224–231 Read Online

ACCESS | Metrics & More | Article Recommendations | Supporting Information

ABSTRACT: Three-dimensional cage-shaped molecules formed from chainlike structures hold potential as unique optoelectronic materials and host compounds. Their optical, structural, and dynamical features are tunable by changes in shape and size. We perform a comparison of these properties for three sizes of strained conjugated [*n.n.n*]carbon nanocages composed of three paraphenylene chains (bridges) of length n = 4, 5, or 6. The exciton intramolecular redistribution occurring during nonradiative relaxation has been explored using nonadiabatic excited-state molecular dynamics. Our results provide atomistic insight into the conformational features associated with the observed red- and blue-shift trends in the absorption and fluorescence spectra, respectively, with increasing nanocage size. Their internal conversion processes involve intramolecular energy transfer that leads to exciton self-trapping on a few phenylene units at the center of a single bridge. The dependence of these dynamical features on the size of the nanocage can be used to tune their host–guest chemical properties and their use for organic electronics and catenane-like applications.

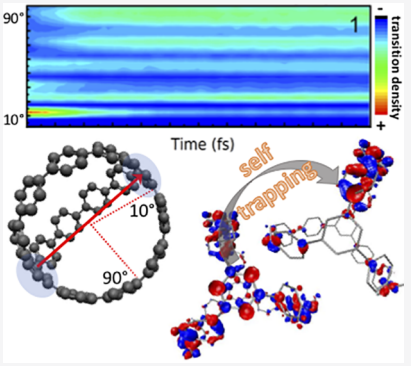

Organic conjugated materials are a broad class of electronically functional chemical compounds used across a variety of technological applications.[1−4] Many of these materials possess tunable optical and electronic properties, offering a way to customize the design of the material for a specific application.[5−10] To this end, establishing structure–property relationships for light absorption and emission features is extremely desirable.[11,12] These relationships can be very complex, as they involve the entire photoexcitation evolution and relaxation via nonadiabatic dynamics that leads to an emissive state. For example, localization of the final fluorescent state following photoexcitation in spiro-linked conjugated polyfluorene stabilizes its light emission.[13] In fact, exciton self-trapping or spatial confinement of the lowest-energy emissive state following photoexcitation has been observed in many conjugated organic systems, particularly those consisting of equivalent chromophores.[13−17] In these systems, exciton migration from an initial state delocalized over two or more equivalent chromophores to a single chromophore unit (or localized site within a single unit) seems to be a ubiquitous feature of the relaxation dynamics. Beyond that, additional hopping between equivalent localized sites on the lowest-energy surface may or may not occur depending on the specific electronic and vibronic couplings.[18]

Exciton migration and self-trapping in circular and curved systems give rise to interesting effects on their optical properties that are not seen in their linear counterparts. The π donors that induce energy transfer in the excited states are typically electron-rich heteroarenes or arenes with electron-donating groups. The discovery that curved oligophenylenes undergo energy transfer in the excited state provides a new option for designing π donor–acceptor molecular systems.[19−21] For example, curved bichromophore molecular polygons (digons) act as unpolarized light absorbers and emitters as a result of bending strain and self-trapping of the emissive state on equivalent vertex units, respectively.[15,22] In ring-shaped cycloparaphenylenes (CPPs), the lowest-energy excited state is forbidden by symmetry. However, strong vibronic coupling during the internal conversion process in CPPs causes excited-state geometry distortions that result in exciton localization and a large transition dipole moment for the emissive state.[23] Therefore, highly efficient fluorescence is observed in large CPPs in violation of the Condon approximation.[24] In both digons and CPPs, the observed effects are size-dependent.

All-benzene carbon nanocages are three-dimensional cage-shaped molecules that combine three equivalent curved [*n*]paraphenylene chains linked together in a single system (see Figure 1a). While CPPs correspond to the shortest sidewall of an armchair carbon nanotube (CNT), carbon

Received: November 10, 2020
Accepted: December 9, 2020
Published: December 16, 2020

https://dx.doi.org/10.1021/acs.jpclett.0c03364
J. Phys. Chem. Lett. 2021, 12, 224–231

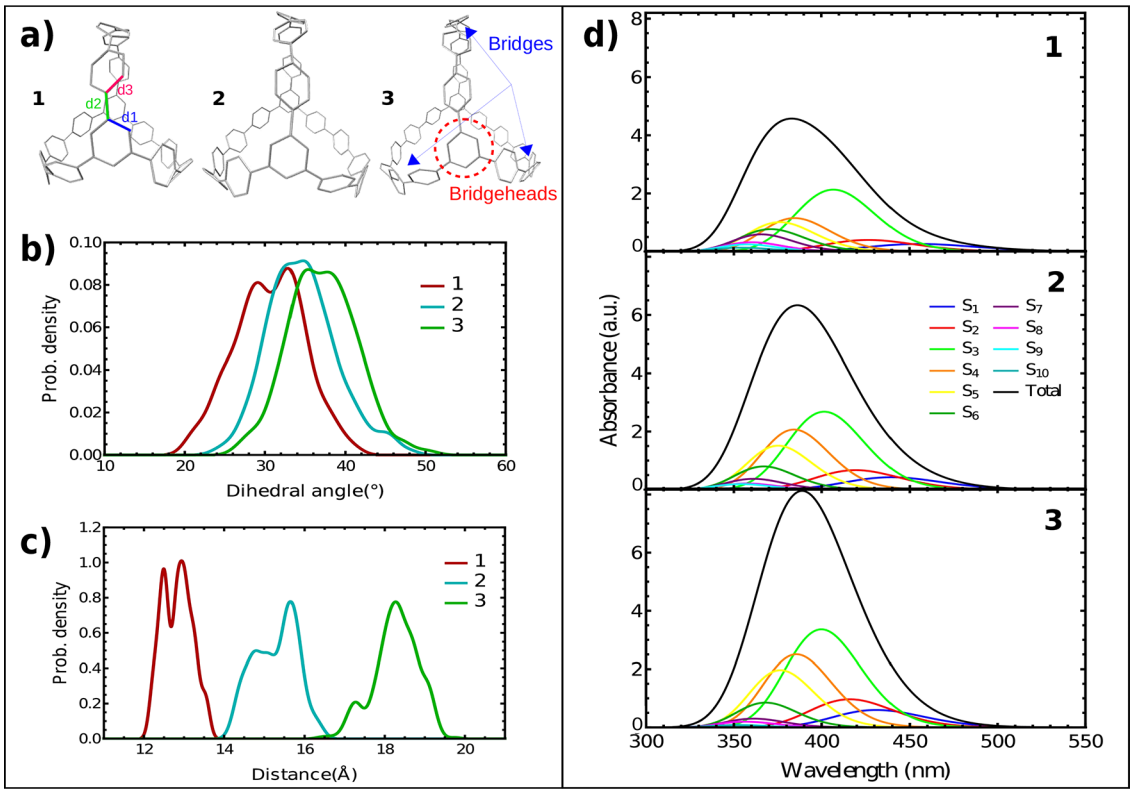

Figure 1. (a) Schematic representation of [*n.n.n*]carbon nanocages **1** (n = 4), **2** (n = 5), and **3** (n = 6) with bridgehead and bridge fragments identified. Bonds d_1, d_2, and d_3 define BLA. (b, c) Probability density distributions of (b) average dihedral angle between neighboring phenyl rings and (c) distance between the two trisubstituted benzene rings (bridgeheads) obtained from 1000 equilibrated ground-state configurations at 300 K for **1**, **2**, and **3**. (d) Simulated absorption spectra at 300 K for **1**, **2**, and **3** showing contributions from different excited states.

nanocages are the analogous structures for branched CNT junctions. They are of interest for their possible use as CNT templates, host−guest chemistry, and catenane-like applications.[25−30] Naturally, one might expect carbon nanocages to exhibit unique optical properties due to the presence of equivalent chromophores and curved chains subject to strain. The synthesis and photophysical properties of [*n.n.n*]carbon nanocages (n = 4, 5, 6) has been previously reported by Itami et al.[31,32] As the size of the carbon nanocage increases (i.e., increasing n), the maximum absorption wavelengths become red-shifted while the fluorescence wavelengths become blue-shifted, which is counterintuitive compared with the properties of conjugated chromophores that typically show concomitant shifts of absorption and emission spectra. Notably, the absorption maxima observed in [*n*]CPPs remain largely independent of the hoop size.[23,33,34]

Here we investigate the exciton evolution in three [*n.n.n*] carbon nanocages (n = 4, 5, 6) following photoexcitation using nonadiabatic excited-state molecular dynamics simulations to model the internal conversion processes.[35,36] The electronic and vibrational energy relaxation connect the absorption and emission properties by providing detailed information on the emissive state. Thus, understanding the relaxation process and electronic energy redistribution in carbon nanocages of different sizes provides valuable insight into optical features and their relationship to the nanocage structure.

We have simulated the photoinduced dynamics of three conjugated [*n.n.n*]carbon nanocages of different sizes denoted as **1** (n = 4), **2** (n = 5), and **3** (n = 6) following Itami et al.,[31,32] shown in Figure 1a. The Nonadiabatic Excited State Molecular Dynamics (NEXMD) code was used in all of the computations, and our modeling protocol is described in Computational Methods. We begin by analyzing the ground-state conformational sampling of each nanocage at 300 K, indicating their differing structural properties. The probability density of the average dihedral angle between neighboring phenylene rings is plotted in Figure 1b. The distributions reveal an increase in the average value of the dihedral angles with increasing nanocage size. This is in agreement with trends previously reported for CPPs and other related bent and curved conjugated molecular systems[5,37−40] and is a consequence of the relaxation of the bending strain of phenylene units due to a reduction of the backbone curvature along longer phenylene bridges. It is interesting to note that the dihedral angle distributions display double peaks. This is due to the presence of two distinct ring types, that is, two benzene-1,3,5-triyl bridgeheads and the remaining rings belonging to the three [*n*]paraphenylene bridges. Bridgehead rings are subjected to greater structural constraints than the others because of their trisubstitution and therefore have relatively lower dihedral angles (Figure S1). Figure 1c shows the probability density distributions for the distance between the two bridgeheads. The width of the distributions increase with the size of the nanocage, indicating an increase in the backbone flexibility. This is confirmed by superpositions of snapshots obtained from the ground-state conformational samplings, which reveal an increase in conformational disorder with increasing size of the cage (Figure S2).

The size of the carbon nanocages also impacts their absorption spectra. This is shown in Figure 1d, where we compare the simulated absorption spectra of **1**, **2**, and **3**. For all of the nanocages, the first two excited states do not present

https://dx.doi.org/10.1021/acs.jpclett.0c03364
J. Phys. Chem. Lett. 2021, 12, 224−231

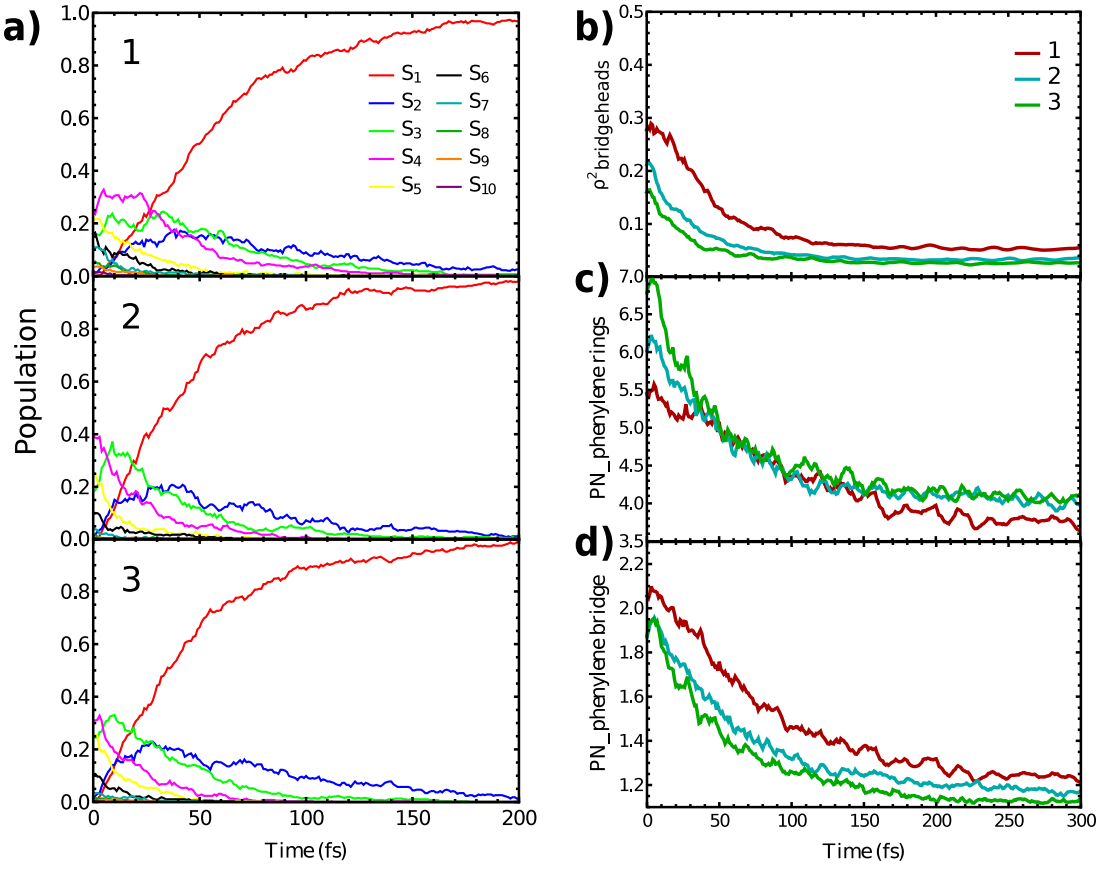

Figure 2. (a) Time evolution of adiabatic electronic state populations (calculated as the fraction of trajectories in each state) during NEXMD simulations of nonadiabatic relaxation dynamics for states S_1−S_{10} participating in the relaxation of carbon nanocages **1**, **2**, and **3**. (b−d) Time evolution of (b) the fraction of transition density localized on the two bridgeheads ($\rho^2_{\text{bridgeheads}}(t)$) (c) the participation number for phenylene rings ($\text{PN}_{\text{phenylene rings}}(t)$), and (d) the participation number for phenylene bridges ($\text{PN}_{\text{phenylene bridges}}(t)$) during NEXMD simulations of carbon nanocages **1**, **2**, and **3**. The photoinduced internal conversion process that takes place in the carbon nanocages can be monitored by following the evolution of the average adiabatic electronic state populations during NEXMD simulations shown in (a). After photoexcitation, the initially excited states (i.e., S_3−S_6) experience an ultrafast relaxation to the S_2 state, which acts as a relatively long-lived intermediate state, and finally the three nanocages completely relax to S_1, an emitting state according to Kasha's rule.[41] This process seems to be more efficient in larger nanocages, as evidenced by the more rapid decay of population from initially excited states and the relatively shorter time to reach S_2 turnover, resulting in an initial slightly faster relaxation.

large oscillator strengths, and the main absorption peaks are dominated by the contributions of the S_3−S_5 states (here and throughout, we adopt the nomenclature of ordering adiabatic states by increasing energy). This is similar to the case of CPP, where the first excited state is strictly optically forbidden at the ground-state geometry by the circular symmetry.[23] Here the selection rules are more relaxed, and the lowest states gain some oscillator strength. The reported experimental absorption maxima of 3.92, 3.86, and 3.81 eV for **1**, **2**, and **3**, respectively,[32] exhibit a slightly increasing red shift as the nanocage size increases. The corresponding simulated absorption maxima are at 3.3, 3.25, and 3.2 eV. Despite the constant red shift with respect to the experimental values, they reproduce the expected ∼0.05 eV red shift displacement with each increase in the nanocage size.

The absorption maxima in carbon nanocages exhibit a noticeable red shift as the cage size increases, in contrast to [*n*]CPPs, which exhibit nearly uniform absorption.[23,33,34] In [*n*]CPPs there seems to be a nearly exact cancellation between red shifts caused by increased conjugation length and blue shifts resulting from less efficient conjugation overlap (i.e., larger dihedrals) between neighboring phenylene rings with increasing *n*, but this is not the case for the carbon nanocages presented here. This could partially be due to the highly constrained bridgehead rings in these [*n.n.n*]carbon nanocages compared with the phenylene units in [*n*]CPPs, leading to smaller effective dihedral angles between the bridgeheads and neighboring rings (Figure S1) and a less efficient corresponding blue shift compensation. This is in agreement with the exciton spatial localization of different excited states on the two bridgeheads (Figure S3), which shows that the states that contribute the most to the main absorption peaks of the nanocages (S_3−S_5) are primarily localized on the bridgeheads for every nanocage size, whereas the lowest-energy S_1 and S_2 states are instead mainly localized on the bridges. Further understanding of the initial exciton spatial localization can be gained through analysis of participation number distributions, $\text{PN}_X(t = 0)$, for each excited state, where X = phenylene rings or phenylene bridges (Figure S3). Considering nanocage **1**, the spatial localization changes among the different excited states and varies significantly as a result of conformational disorder introduced by thermal fluctuations. While S_1 is localized on a few phenylene rings ($\text{PN}_{\text{phenylene rings}}(t = 0) \approx 4$−$6$) involving only one or two of the bridges ($\text{PN}_{\text{phenylene bridges}}(t = 0) \approx 1$−$2$), the S_2 and S_3 states are delocalized among several phenylene rings that can be spread across the three phenylene bridges.

https://dx.doi.org/10.1021/acs.jpclett.0c03364
J. Phys. Chem. Lett. 2021, 12, 224−231

Finally, higher excited states ($S_{\geq 4}$) involve fewer phenylene units than S_1 but are delocalized on different phenylene bridges. Similar results are observed for nanocages **2** and **3**.

According to our previous analysis of the exciton spatial localization of different excited states (Figure S3), the initial excitation, which involves a range of states (S_3−S_6) because of the thermal fluctuations across the ensemble of initial configurations, is characterized by larger fractions of transition densities in the bridgeheads compared with lower-energy states, which are primarily localized on the phenylene bridges. Therefore, intramolecular energy transfer from bridgeheads to phenylene bridges is expected to occur during the internal conversion. This is confirmed by following the evolution of the average fraction of transition density localized on the bridgeheads during NEXMD simulations, which is plotted in Figure 2b. The initial exciton localization on the bridgeheads is significantly reduced during the course of energy relaxation for the three nanocages, a process that is more pronounced for the smaller nanocages. In addition, the evolution of the participation numbers for the phenylene rings and the phenylene bridges, plotted in Figure 2c,d, respectively, shows that all three nanocages experience exciton self-trapping that localizes the exciton on only a few (four) phenylene units ($PN_{\text{phenylene rings}}(t = 300\ \text{fs}) \approx 4$) concentrated on a single phenylene bridge ($PN_{\text{phenylene bridges}}(t = 300\ \text{fs}) \approx 1.2$). More specifically, the exciton experiences an ultrafast migration toward the *center* of the phenylene bridge, as revealed by the change in angular displacement of the transition density within the carbon nanocages (Figure S4).

As we have shown, the intramolecular exciton migration during internal conversion leads to exciton self-trapping on the center of one of the phenylene bridges. In order to track the exciton exchange among the different phenylene bridges, we have classified the phenylene bridges according to their final relative fractions of transition density as high (H), middle (M), and low (L). Following this classification, Figure 3 displays the evolution of different electronic and structural features for each of the phenylene bridges in nanocage **1**. First, the change in $\rho^2_{\text{phenylene bridges}}$ (Figure 3a) indicates that the phenylene bridge where the exciton is finally trapped (H) is not related to the initial excitation since all of the bridges share the same initial density value, $\rho^2_{\text{phenylene bridges}}(t = 0) \approx 0.25$. Next, we analyze the structural changes during the electronic relaxation, specifically the average dihedral angle between neighboring phenylene units on the bridges and the average bond length alternation (BLA) along the bridges. BLA reflects the inhomogeneity in the distribution of the π-conjugated electrons, and it is defined as $d_1 - \frac{2}{3}d_2 - \frac{1}{3}d_3$, where d_1, d_2, and d_3 are consecutive bond distances labeled in Figure 1a. The H bridge experiences a larger planarization, i.e., lower values of dihedral angles between neighboring rings (Figure 3b), and lower BLA values (Figure 3c) than the M and L bridges. Both planarization and decreased BLA are characteristic signatures of exciton self-trapping in excited-state dynamics.[13,37,42−46] Both the extent of planarization and the decrease in BLA become more and more reduced for larger nanocage sizes (see Figures S5 and S6 for the corresponding values for nanocages **2** and **3**, respectively). We obtained final average dihedral angle values of ∼10°, 20°, and 24° and final average BLA values of ∼0.03, 0.035, and 0.04 Å for **1**, **2**, and **3**, respectively. Therefore, the efficiency of the exciton self-trapping decreases with increasing size of the nanocage given a concomitant increase of conjugation.

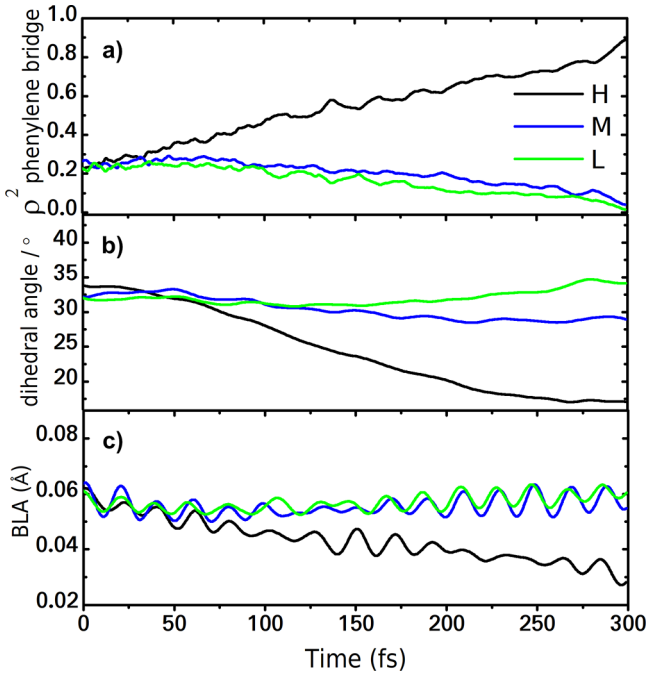

Figure 3. Time evolution of different electronic and structural features for high (H), middle (M), and low (L) phenylene bridges in carbon nanocage **1** during NEXMD simulations. H, M, and L correspond to phenylene bridges with decreasing final values of $\rho^2_{\text{phenylene bridges}}$. (a) Fraction of transition density. (b) Average dihedral angle between neighboring phenylene bridge units. (c) Average bond length alternation along the bridge.

Previous studies performed on CPPs[38] point out that planarization in the excited states leads to larger Stokes shifts in smaller CPPs as a result of the increased structural relaxation in the S_1 state. This is also the case for carbon nanocages. Even though the final time of our simulations was only 300 fs, we observed that the simulated emission spectra of the nanocages (Figure S7) are blue-shifted for the larger cage sizes, having emission peak maxima of 520, 500, and 480 nm for **1**, **2**, and **3**, respectively. This corresponds to an increase in Stokes shift for the smaller nanocages. The blue shift per nanocage, ordered by increasing size, was ∼0.7−0.9 eV. That is, the progressive planarization and decreasing BLA stabilize the lowest-energy S_1 state responsible for the final emission properties. This is in good agreement with previous calculations that indicate an increase in the HOMO−LUMO gap (main contribution to the S_1 state) as the size of the nanocage increases.[32]

In conclusion, we have investigated the photoinduced dynamics and intramolecular exciton energy transfer of three conjugated [*n.n.n*]carbon nanocages of different sizes (n = 4, 5, 6) using nonadiabatic excited-state molecular dynamics. The nonradiative relaxation processes are found to be similar in all of the nanocages, becoming only slightly faster with increasing cage size. Our simulations reproduce the spectral trends observed experimentally and allow us to explain both the slightly increasing red shift of the absorption and the blue shift of the emission with increasing cage size. Notably, the absorbing and emitting states have different electronic properties and spatial localizations of the electronic wave functions in all of the nanocages. The absorption red shift seems to be related to the dominant contribution of relatively

https://dx.doi.org/10.1021/acs.jpclett.0c03364
J. Phys. Chem. Lett. 2021, 12, 224−231

more constrained bridgehead benzenes hosting the electronic states responsible for the main absorption peaks. In contrast, the emission blue shift is associated with additional stabilization of the lowest-energy S_1 state responsible for emission. The S_1 stabilization effect is enhanced in smaller cages, thus leading to larger Stokes shifts in smaller cages and the progressive emission blue shift for larger cages. We found that the internal conversion processes of carbon nanocages, which connect the absorption and emission properties, involve an intramolecular energy transfer from bridgeheads to phenylene bridges. The three nanocages experience exciton self-trapping that localizes the exciton on only a few phenylene units at the center of a single phenylene bridge. The efficiency of the exciton self-trapping decreases for larger nanocages, as evidenced by different torsional and bond-length relaxation of the excited-state geometry.

Nanocages stand out among carbon-based nanostructures regarding their potential applications for energy storage and conversion, especially because of their tunable electronic structure.[19,29,30,47] The strong dependence of the properties of carbon nanocages (e.g., pore distribution, specific surface area, and electronic structure) on the synthetic conditions and templates emphasizes the importance of first-principles theoretical modeling of these multifunctional materials. In particular, predictions based on nanosized symmetric models may be regarded as upper bounds of the functionalities of the real carbon nanocages, especially for properties relying on collective electron response (i.e., the properties of the nanostructure depend sensitively on the particular three-dimensional assembly of the cages). Therefore, the results of the present simulations more closely reflect reflect more closely the properties of highly ordered assemblies of carbon nanocages, which have been reported recently and exhibit superior performance compared with randomly packed structures.[47] On the one hand, the present simulations enable an assessment of the influence of the geometry and electronic structure of these molecules on the exciton localization and spectroscopic properties, which ultimately determine the performance of assemblies of carbon-based nanocages for different applications. On the other hand, the computational efficiency of NEXMD simulations allows current limitations of atomistic simulations to be overcome, bridging the gap between the nowadays computationally affordable and the experimentally relevant molecules. Our atomistic description of the photoinduced intrachain energy transfer and exciton self-trapping in carbon nanocages, as building blocks of branched multiterminal single-wall carbon nanotube junctions, establishes the relationship between nanocage size, structural, and chemical features with their dynamic motions, exciton spatial localization, π conjugation, and optoelectronic properties.

These relationships can guide future functionalization that may potentially increase the specificity of their host–guest chemistry and impact their use in organic electronics and catenane-like applications[29,30] in a desired way.

COMPUTATIONAL METHODS

Simulation Details. The Nonadiabatic Excited State Molecular Dynamics (NEXMD) package[48,49] has been specifically developed to simulate the photoinduced nonadiabatic electronic and vibrational energy relaxation and redistribution in large multichromophoric conjugated molecules involving multiple coupled electronic excited states. The code combines the surface hopping algorithm[50,51] with "on the fly" calculations of excited-state energies, gradients, and vibronic couplings using the collective electronic oscillator (CEO) approach[52] at the configuration interaction singles (CIS) level with the semiempirical AM1 Hamiltonian.[53]

Within the CEO formalism, transition energies, excited-state gradients, single-electron density matrices, dipole moments, and other relevant quantities are cast in terms of the transition density matrices.[35] Thus, both the optical response and the dynamic exciton localization properties are computed at the same level of theory, and intuitively we expect these observables to be described with similar accuracy. Moreover, previous NEXMD simulations yield spectra and exciton migration properties in good correspondence with experimental results across a variety of conjugated molecules undergoing quite distinct exciton relaxation pathways,[35] which is very encouraging with regard to the application of the present methodology to the simulation of the photoinduced dynamics of carbon nanocages. It has been successfully applied to simulate the photoinduced dynamics of the family of [n]CPPs and other related nanohoops,[5,23,37,46] providing good agreement with more accurate quantum-chemical calculations. Previous NEXMD simulations were able to associate the efficient fluorescence in large [n]CPP hoops with the exciton self-trapping due to strong vibronic coupling, breaking the Condon approximation and overriding the optical selection rules.[23] In this way, previous works validate NEXMD simulations as an accurate level of theory to describe the intramolecular electronic and vibrational energy relaxation and redistribution in cyclic paraphenylene chromophores.[35]

The NEXMD simulations were performed on the series of conjugated [$n.n.n$]carbon nanocages with n = 4, 5, and 6, denoted as **1**, **2**, and **3**, respectively (Figure 1a). Initial conditions were collected from equilibrated ground-state conformational sampling obtained from 30 individual 3 ns adiabatic ground-state molecular dynamics simulations at 300 K with a Langevin friction coefficient γ = 20.0 ps^{-1} and a classical time step of 0.5 fs. The initial configurations for these 30 simulations were provided by a previous 3 ns ground-state trajectory at 500 K. Absorption spectra were calculated by collecting vertical transition energies and oscillator strengths calculated from 1000 equilibrated ground-state conformational samplings at 300 K and applying a Gaussian line shape with 0.1 eV broadening. For each nanocage, 400 independent non-adiabatic trajectories were propagated at constant energy using classical time steps of 0.1 fs for nuclei and 0.025 fs for electronic coefficients. These simulations were started by vertical excitation to an initial excited state selected according to a Franck–Condon window given by $g_\alpha = \exp[-T^2(E_{\text{laser}} - \Omega_\alpha)^2]$, where Ω_α represents the energy of the αth excited state and E_{laser} corresponds to the energy of a Gaussian laser pulse $f(t) = \exp(-t^2/2T^2)$ centered at 3.3 eV, which approximately corresponds to the maximum of the simulated absorption spectra for the three systems (Figure 1d). A value of T^2 = 42.5 fs, corresponding to a full width at half-maximum (fwhm) of 100 fs, was considered. Specific treatments of decoherence[54] and trivial unavoided crossings[55] have been applied. More details about the NEXMD approach, implementation, and testing parameters can be found elsewhere[48,49,56]

Analysis of Exciton Properties. Within the NEXMD framework, the time evolution of the spatial exciton localization is analyzed in terms of $\boldsymbol{\rho}^{g\alpha}(t)$, the transition density matrix between a ground state g and an excited state α with adiabatic wave function ϕ_α: $(\rho^{g\alpha}(t))_{nm} \equiv \langle \phi_\alpha | c_m^+ c_n | \phi_g \rangle$, where c_m^+ (c_n) is

https://dx.doi.org/10.1021/acs.jpclett.0c03364
J. Phys. Chem. Lett. 2021, 12, 224–231

the creation (annihilation) electronic operator and n and m index atomic orbital (AO) basis functions. Diagonal elements $(\rho^{g\alpha}(t))_{nn}$ are relevant to the changes in the distribution of electronic density induced by photoexcitation to state α.[49,57] According to the normalization condition $\sum_{nm}((\rho^{g\alpha})_{nm})^2 = 1$, the fraction of transition density localized on a specific fragment X of the molecular system can be calculated as

$$(\rho^{g\alpha}(t))_X^2 = \sum_{n_A m_A} ((\rho^{g\alpha})_{n_A m_A})^2 \quad (1)$$

where the subindex A indicates AOs of atoms constituting the selected fragment X of the molecule. In the present work, the exciton spatial localization has been analyzed by dividing the molecule into the following fragments: individual phenylene rings, the two trisubstituted benzene rings (bridgeheads), and the three paraphenylene bridges (see Figure 1a), considered both together and individually. The extent of the exciton (de)localization among the different fragments can be measured using the participation number, defined as

$$PN_X(t) = \left[\sum_X^M ((\rho^{g\alpha}(t))_X^2)^2\right]^{-1} \quad (2)$$

where M is the total number of fragments into which the molecule is partitioned. $PN_X(t) \approx 1$ indicates complete localization of $\rho^{g\alpha}(t)$ on fragment X, while $PN_X(t) \approx M$ indicates full delocalization of $\rho^{g\alpha}(t)$ among the M equivalent fragments. Herein we have considered different types of equivalent fragments. Therefore, according to Figure 1a, M = (14 (**1**), 17 (**2**), 20 (**3**)) for X = phenylene rings, M = 2 for X = bridgeheads, and M = 3 for X = bridges.

■ ASSOCIATED CONTENT

Supporting Information

The Supporting Information is available free of charge at https://pubs.acs.org/doi/10.1021/acs.jpclett.0c03364.

Comparison of bridgehead and bridge dihedral angles (Figure S1); sampled molecular configurations (Figure S2); spatial localization for different excited states (Figure S3); change in the angular distribution of the transition density (Figure S4); transition density, dihedral angles, and BLA for H, M, and L bridges in **2** (Figure S5); transition density, dihedral angles, and BLA for H, M, and L bridges in **3** (Figure S6); simulated emission spectra (Figure S7) (PDF)

■ AUTHOR INFORMATION

Corresponding Author

Sebastian Fernandez-Alberti − *Departamento de Ciencia y Tecnologia, Universidad Nacional de Quilmes/CONICET, B1876BXD Bernal, Argentina;* orcid.org/0000-0002-0916-5069; Email: sfalberti@gmail.com

Authors

Beatriz Rodríguez-Hernández − *Departamento de Ciencia y Tecnologia, Universidad Nacional de Quilmes/CONICET, B1876BXD Bernal, Argentina*

Tammie Nelson − *Physics and Chemistry of Materials, Theoretical Division, Los Alamos National Laboratory, Los Alamos, New Mexico 87545, United States;* orcid.org/0000-0002-3173-5291

Nicolas Oldani − *Departamento de Ciencia y Tecnologia, Universidad Nacional de Quilmes/CONICET, B1876BXD Bernal, Argentina*

Aliezer Martínez-Mesa − *Departamento de Ciencia y Tecnologia, Universidad Nacional de Quilmes/CONICET, B1876BXD Bernal, Argentina; DynAMoS (Dynamical processes in Atomic and Molecular Systems), Facultad de Física, Universidad de La Habana, La Habana 10400, Cuba*

Llinersy Uranga-Piña − *Departamento de Ciencia y Tecnologia, Universidad Nacional de Quilmes/CONICET, B1876BXD Bernal, Argentina; DynAMoS (Dynamical processes in Atomic and Molecular Systems), Facultad de Física, Universidad de La Habana, La Habana 10400, Cuba*

Yasutomo Segawa − *Graduate School of Science, Nagoya University, Nagoya 464-8602, Japan; JST, ERATO, Itami Molecular Nanocarbon Project, Nagoya University, Nagoya 464-8602, Japan; Institute for Molecular Science, Okazaki 444-8787, Japan; Department of Structural Molecular Science, SOKENDAI (The Graduate University for Advanced Studies), Okazaki 444-8787, Japan;* orcid.org/0000-0001-6439-8546

Sergei Tretiak − *Physics and Chemistry of Materials, Theoretical Division, Los Alamos National Laboratory, Los Alamos, New Mexico 87545, United States; Center for Integrated Nanotechnologies, Los Alamos National Laboratory, Los Alamos, New Mexico 87545, United States;* orcid.org/0000-0001-5547-3647

Kenichiro Itami − *Graduate School of Science, Nagoya University, Nagoya 464-8602, Japan; JST, ERATO, Itami Molecular Nanocarbon Project and Institute of Transformative Bio-Molecules (WPI-ITbM), Nagoya University, Nagoya 464-8602, Japan;* orcid.org/0000-0001-5227-7894

Complete contact information is available at: https://pubs.acs.org/10.1021/acs.jpclett.0c03364

Notes

The authors declare no competing financial interest.

■ ACKNOWLEDGMENTS

The work at Los Alamos National Laboratory (LANL) was supported by the LANL Directed Research and Development Funds (LDRD) and performed in part at the Center for Nonlinear Studies (CNLS) and the Center for Integrated Nanotechnologies (CINT), a U.S. Department of Energy Office of Science User Facility at LANL. S.F.-A. was supported by CONICET, UNQ, and ANPCyT (PICT-2018-02360). This research used resources provided by the LANL Institutional Computing (IC) Program. LANL is operated by Triad National Security, LLC, for the National Nuclear Security Administration of the U.S. Department of Energy (Contract 89233218NCA000001).

■ REFERENCES

(1) Wang, M.; Baek, P.; Akbarinejad, A.; Barker, D.; Travas-Sejdic, J. Conjugated Polymers and Composites for Stretchable Organic Electronics. *J. Mater. Chem. C* **2019**, *7*, 5534−5552.

(2) Ostroverkhova, O. Organic Optoelectronic Materials: Mechanisms and Applications. *Chem. Rev.* **2016**, *116*, 13279−13412.

(3) Zuo, G.; Abdalla, H.; Kemerink, M. Conjugated Polymer Blends for Organic Thermoelectrics. *Adv. Elec. Mater.* **2019**, *5*, 1800821.

(4) Kimpel, J.; Michinobu, T. Conjugated Polymers for Functional Applications: Lifetime and Performance of Polymeric Organic

Semiconductors in Organic Field-Effect Transistors. *Polym. Int.* **2020**, DOI: 10.1002/pi.6020.
(5) Rodriguez-Hernandez, B.; Ondarse-Alvarez, D.; Oldani, N.; Martinez-Mesa, A.; Uranga-Piña, Ll.; Tretiak, S.; Fernandez-Alberti, S. Modification of Optical Properties and Excited-State Dynamics by Linearizing Cyclic Paraphenylene Chromophores. *J. Phys. Chem. C* **2018**, *122*, 16639−16648.
(6) Huix-Rotllant, M.; Tamura, H.; Burghardt, I. Concurrent Effects of Delocalization and Internal Conversion Tune Charge Separation at Regioregular Polythiophene−Fullerene Heterojunctions. *J. Phys. Chem. Lett.* **2015**, *6*, 1702−1708.
(7) Ji, W.; Xue, B.; Bera, S.; Guerin, S.; Liu, Y.; Yuan, H.; Li, Q.; Yuan, C.; Shimon, L. J. W.; Ma, Q.; et al. Tunable Mechanical and Optoelectronic Properties of Organic Cocrystals by Unexpected Stacking Transformation from H- to J- and X-Aggregation. *ACS Nano* **2020**, *14*, 10704−10715.
(8) Liu, D.; Yang, L.; Wu, Y.; Wang, X.; Zeng, Y.; Han, G.; Yao, H.; Li, S.; Zhang, S.; Zhang, Y.; et al. Tunable Electron Donating and Accepting Properties Achieved by Modulating the Steric Hindrance of Side Chains in A−D−A Small-Molecule Photovoltaic Materials. *Chem. Mater.* **2018**, *30*, 619−628.
(9) Yoshino, K.; Takeda, H.; Kasano, M.; Satoh, S.; Matsui, T.; Ozaki, R.; Fujii, A.; Ozaki, M.; Kose, A. Novel Tunable Optical Properties of Liquid Crystals, Conjugated Molecules and Polymers in Nanoscale Periodic Structures as Photonic Crystals. *Macromol. Symp.* **2004**, *212*, 179−190.
(10) Guerlin, A.; Dumur, F.; Dumas, E.; Miomandre, F.; Wantz, G.; Mayer, C. R. Tunable Optical Properties of Chromophores Derived from Oligo(*p*-phenylene vinylene). *Org. Lett.* **2010**, *12*, 2382−2385.
(11) Li, Y.; Vamvounis, G.; Holdcroft, S. Tuning Optical Properties and Enhancing Solid-State Emission of Poly(thiophene)s by Molecular Control: A Postfunctionalization Approach. *Macromolecules* **2002**, *35*, 6900−6906.
(12) Portone, A.; Ganzer, L.; Branchi, F.; Ramos, R.; Caldas, M. J.; Pisignano, D.; Molinari, E.; Cerullo, G.; Persano, L.; Prezzi, D.; Virgili, T. Tailoring Optical Properties and Stimulated Emission in Nanostructured Polythiophene. *Sci. Rep.* **2019**, *9*, 7370.
(13) Ondarse-Alvarez, D.; Oldani, N.; Tretiak, S.; Fernandez-Alberti, S. Computational Study of Photoexcited Dynamics in Bichromophoric Cross-Shaped Oligofluorene. *J. Phys. Chem. A* **2014**, *118*, 10742−10753.
(14) Alfonso Hernandez, L.; Nelson, T.; Tretiak, S.; Fernandez-Alberti, S. Photoexcited Energy Transfer in a Weakly Coupled Dimer. *J. Phys. Chem. B* **2015**, *119*, 7242−7252.
(15) Ondarse-Alvarez, D.; Nelson, T.; Lupton, J. M.; Tretiak, S.; Fernandez-Alberti, S. Let Digons be Bygones: The Fate of Excitons in Curved π-Systems. *J. Phys. Chem. Lett.* **2018**, *9*, 7123−7129.
(16) Ondarse-Alvarez, D.; Komurlu, S.; Roitberg, A. E.; Pierdominici-Sottile, G.; Tretiak, S.; Fernandez-Alberti, S.; Kleiman, V. D. Ultrafast Electronic Energy Relaxation in a Conjugated Dendrimer Leading to Inter-Branch Energy Redistribution. *Phys. Chem. Chem. Phys.* **2016**, *18*, 25080−25089.
(17) Alfonso Hernandez, L.; Nelson, T.; Gelin, M. F.; Lupton, J. M.; Tretiak, S.; Fernandez-Alberti, S. Interference of Interchromophoric Energy-Transfer Pathways in π-Conjugated Macrocycles. *J. Phys. Chem. Lett.* **2016**, *7*, 4936−4944.
(18) Nelson, T. R.; Ondarse-Alvarez, D.; Oldani, N.; Rodriguez-Hernandez, B.; Alfonso-Hernandez, L.; Galindo, J. F.; Kleiman, V. D.; Fernandez-Alberti, S.; Roitberg, A. E.; Tretiak, S. Coherent Exciton-Vibrational Dynamics and Energy Transfer in Conjugated Organics. *Nat. Commun.* **2018**, *9*, 2316.
(19) Kuwabara, T.; Orii, J.; Segawa, Y.; Itami, K. Curved Oligophenylenes as Donors in Shape-Persistent Donor−Acceptor Macrocycles with Solvatofluorochromic Properties. *Angew. Chem., Int. Ed.* **2015**, *54*, 9646−9649.
(20) Lovell, T. C.; Garrison, Z. R.; Jasti, R. Synthesis, Characterization, and Computational Investigation of Bright Orange-Emitting Benzothiadiazole [10]Cycloparaphenylene. *Angew. Chem., Int. Ed.* **2020**, *59*, 14363−14367.
(21) Van Raden, J. M.; Darzi, E. R.; Zakharov, L. N.; Jasti, R. Synthesis and Characterization of a Highly Strained Donor−Acceptor Nanohoop. *Org. Biomol. Chem.* **2016**, *14*, 5721−5727.
(22) Wilhelm, P.; Vogelsang, J.; Poluektov, G.; Schönfelder, N.; Keller, T. J.; Jester, S.-S.; Höger, S.; Lupton, J. M. Molecular Polygons Probe the Role of Intramolecular Strain in the Photophysics of π-Conjugated Chromophores. *Angew. Chem., Int. Ed.* **2017**, *56*, 1234−1238.
(23) Adamska, L.; Nayyar, I.; Chen, H.; Swan, A. K.; Oldani, N.; Fernandez-Alberti, S.; Golder, M. R.; Jasti, R.; Doorn, S. K.; Tretiak, S. Self-Trapping of Excitons, Violation of Condon Approximation, and Efficient Fluorescence in Conjugated Cycloparaphenylenes. *Nano Lett.* **2014**, *14*, 6539−6546.
(24) Condon, E. U. Nuclear Motion Associated with Electron Transitions in Diatomic Molecules. *Phys. Rev.* **1928**, *32*, 858−872.
(25) Hof, F.; Craig, S. L.; Nuckolls, C.; Rebek, J., Jr. Molecular Encapsulation. *Angew. Chem., Int. Ed.* **2002**, *41*, 1488−1508.
(26) Mastalerz, M. Shape-Persistent Organic Cage Compounds by Dynamic Covalent Bond Formation. *Angew. Chem., Int. Ed.* **2010**, *49*, 5042−5053.
(27) Fujita, M.; Tominaga, M.; Hori, A.; Therrien, B. Coordination Assemblies from a Pd(II)-Cornered Square Complex. *Acc. Chem. Res.* **2005**, *38*, 369−378.
(28) Zhang, D.; Nie, Y.; Saha, M. L.; He, Z.; Jiang, L.; Zhou, Z.; Stang, P. J. Photoreversible [2] Catenane via the Host-Guest Interactions between a Palladium Metallacycle and beta-Cyclodextrin. *Inorg. Chem.* **2015**, *54*, 11807−11812.
(29) Segawa, Y.; Levine, D. R.; Itami, K. Topologically Unique Molecular Nanocarbons. *Acc. Chem. Res.* **2019**, *52*, 2760−2767.
(30) Segawa, Y.; Kuwayama, M.; Hijikata, Y.; Fushimi, M.; Nishihara, T.; Pirillo, J.; Shirasaki, J.; Kubota, N.; Itami, K. Topological Molecular Nanocarbons: All-Benzene Catenane and Trefoil Knot. *Science* **2019**, *365*, 272−276.
(31) Matsui, K.; Segawa, Y.; Namikawa, T.; Kamada, K.; Itami, K. Synthesis and Properties of All-Benzene Carbon Nanocages: A Junction Unit of Branched Carbon Nanotubes. *Chem. Sci.* **2013**, *4*, 84−88.
(32) Matsui, K.; Segawa, Y.; Itami, K. All-Benzene Carbon Nanocages: Size-Selective Synthesis, Photophysical Properties, and Crystal Structure. *J. Am. Chem. Soc.* **2014**, *136*, 16452−16458.
(33) Segawa, Y.; Fukazawa, A.; Matsuura, S.; Omachi, H.; Yamaguchi, S.; Irle, S.; Itami, K. Combined Experimental and Theoretical Studies on the Photophysical Properties of Cycloparaphenylenes. *Org. Biomol. Chem.* **2012**, *10*, 5979−5984.
(34) Lewis, S. Cycloparaphenylenes and Related Nanohoops. *Chem. Soc. Rev.* **2015**, *44*, 2221−2304.
(35) Nelson, T.; White, A. J.; Bjorgaard, J. A.; Sifain, A. E.; Zhang, Y.; Nebgen, B.; Fernandez-Alberti, S.; Mozyrsky, D.; Roitberg, A. E.; Tretiak, S. Non-adiabatic Excited-State Molecular Dynamics: Theory and Applications for Modeling Photophysics in Extended Molecular Materials. *Chem. Rev.* **2020**, *120*, 2215−2287.
(36) Nelson, T.; Fernandez-Alberti, S.; Roitberg, A. E.; Tretiak, S. Nonadiabatic Excited-State Molecular Dynamics: Modeling Photophysics in Organic Conjugated Materials. *Acc. Chem. Res.* **2014**, *47*, 1155−1164.
(37) Oldani, N.; Doorn, S. K.; Tretiak, S.; Fernandez-Alberti, S. Photoinduced Dynamics in Cycloparaphenylenes: Planarization, Electron−Phonon Coupling, Localization and Intra-Ring Migration of the Electronic Excitation. *Phys. Chem. Chem. Phys.* **2017**, *19*, 30914−30924.
(38) Jasti, R.; Bhattacharjee, J.; Neaton, J.; Bertozzi, C. Synthesis, Characterization, and Theory of [9]-, [12]-, and [18]-Cycloparaphenylene: Carbon Nanohoop Structures. *J. Am. Chem. Soc.* **2008**, *130*, 17646−17647.
(39) Segawa, Y.; Omachi, H.; Itami, K. Theoretical Studies on the Structures and Strain Energies of Cycloparaphenylenes. *Org. Lett.* **2010**, *12*, 2262.
(40) Sundholm, D.; Taubert, S.; Pichierri, F. Calculation of Absorption and Emission Spectra of [*n*]Cycloparaphenylenes: The

https://dx.doi.org/10.1021/acs.jpclett.0c03364
J. Phys. Chem. Lett. 2021, 12, 224−231

Reason for the Large Stokes Shift. *Phys. Chem. Chem. Phys.* **2010**, *12*, 2751−2757.
(41) Kasha, M. Characterization of Electronic Transitions in Complex Molecules. *Discuss. Faraday Soc.* **1950**, *9*, 14−19.
(42) Clark, J.; Nelson, T.; Tretiak, S.; Cirmi, G.; Lanzani, G. Femtosecond Torsional Relaxation. *Nat. Phys.* **2012**, *8*, 225−231.
(43) Tretiak, S.; Saxena, A.; Martin, R. L.; Bishop, A. R. Conformational Dynamics of Photoexcited Conjugated Molecules. *Phys. Rev. Lett.* **2002**, *89*, 097402.
(44) Karabunarliev, S.; Baumgarten, M.; Bittner, E. R.; Mullen, K. Rigorous Franck Condon Absorption and Emission Spectra of Conjugated Oligomers from Quantum Chemistry. *J. Chem. Phys.* **2000**, *113*, 11372−11381.
(45) Franco, I.; Tretiak, S. Electron-Vibrational Dynamics of Photoexcited Polyfluorenes. *J. Am. Chem. Soc.* **2004**, *126*, 12130−12140.
(46) Franklin-Mergarejo, R.; Alvarez, D. O.; Tretiak, S.; Fernandez-Alberti, S. Carbon Nanorings with Inserted Acenes: Breaking Symmetry in Excited State Dynamics. *Sci. Rep.* **2016**, *6*, 31253.
(47) Wu, Q.; Yang, L.; Wang, X.; Hu, Z. Carbon?Based Nanocages: A New Platform for Advanced Energy Storage and Conversion. *Adv. Mater.* **2019**, *32*, 1904177.
(48) Nelson, T.; Fernandez-Alberti, S.; Chernyak, V.; Roitberg, A. E.; Tretiak, S. Nonadiabatic Excited-State Molecular Dynamics Modeling of Photoinduced Dynamics in Conjugated Molecules. *J. Phys. Chem. B* **2011**, *115*, 5402−5414.
(49) Malone, W.; Nebgen, B.; White, A.; Zhang, Y.; Song, H.; Bjorgaard, J. A.; Sifain, A. E.; Rodriguez-Hernandez, B.; Freixas, V. M.; Fernandez-Alberti, S.; et al. NEXMD Software Package for Nonadiabatic Excited State Molecular Dynamics Simulations. *J. Chem. Theory Comput.* **2020**, *16*, 5771−5783.
(50) Tully, J. Molecular Dynamics with Electronic Transitions. *J. Chem. Phys.* **1990**, *93*, 1061−1071.
(51) Hammes-Schiffer, S.; Tully, J. C. Proton Transfer in Solution: Molecular Dynamics with Quantum Transitions. *J. Chem. Phys.* **1994**, *101*, 4657−4667.
(52) Tretiak, S.; Mukamel, S. Density Matrix Analysis and Simulation of Electronic Excitations in Conjugated and Aggregated Molecules. *Chem. Rev.* **2002**, *102*, 3171−3212.
(53) Dewar, M. J. S.; Zoebisch, E. G.; Healy, E. F.; Stewart, J. J. P. The Development and Use of Quantum Mechanical Molecular Models. 76. AMI: A New General Purpose Quantum Mechanical Molecular Model. *J. Am. Chem. Soc.* **1985**, *107*, 3902.
(54) Nelson, T.; Fernandez-Alberti, S.; Roitberg, A. E.; Tretiak, S. Nonadiabatic Excited-State Molecular Dynamics: Treatment of Electronic Decoherence. *J. Chem. Phys.* **2013**, *138*, 224111.
(55) Fernandez-Alberti, S.; Roitberg, A.; Nelson, T.; Tretiak, S. Identification of Unavoided Crossings in Nonadiabatic Photoexcited Dynamics Involving Multiple Electronic States in Polyatomic Conjugated Molecules. *J. Chem. Phys.* **2012**, *137*, 014512.
(56) Nelson, T.; Fernandez-Alberti, S.; Chernyak, V.; Roitberg, A.; Tretiak, S. Nonadiabatic Excited-State Molecular Dynamics: Numerical Tests of Convergence and Parameters. *J. Chem. Phys.* **2012**, *136*, 054108.
(57) Wu, C.; Malinin, S. V.; Tretiak, S.; Chernyak, V. Y. Exciton Scattering and Localization in Branched Dendrimeric Structures. *Nat. Phys.* **2006**, *2*, 631−635.

https://dx.doi.org/10.1021/acs.jpclett.0c03364
J. Phys. Chem. Lett. 2021, 12, 224−231